Spectroscopy and population decay of a van der Waals gap state in layered $TiSe_2$

M. Wiesenmayer,[1,*] S. Hilgenfeldt,[1] S. Mathias,[2,3] F. Steeb,[3] T. Rohwer,[1] and M. Bauer[1]
[1]*Institut für Experimentelle und Angewandte Physik, Christian-Albrechts-Universität zu Kiel, 24118 Kiel, Germany*
[2]*JILA, University of Colorado and National Institute of Standards and Technology, Boulder, Colorado 80309-0440, USA*
[3]*Department of Physics and Research Center OPTIMAS, University of Kaiserslautern, 67663 Kaiserslautern, Germany*
(Received 11 September 2009; revised manuscript received 19 June 2010; published 15 July 2010)

Two-photon photoemission (2PPE) spectroscopy is used to map the momentum-dependent energy distribution of unoccupied bands in the layered $1T$-$TiSe_2$ transition-metal dichalcogenide compound. A comparison of the experimental results with previous calculations based on the local-density functional approach enables us to identify the second Ti $3d$ conduction band and a localized unoccupied state that we assign to the presence of excess titanium atoms in the van der Waals gap of the crystal. Time-resolved 2PPE measurements show clear differences in the lifetime between the two states, indicative for the decoupling of the Ti excess atoms from the bulk electronic structure.

DOI: 10.1103/PhysRevB.82.035422 PACS number(s): 79.60.−i, 78.47.−p, 73.20.Hb

I. INTRODUCTION

The compound class of the layered transition-metal dichalcogenides (TMDC) is considered a model system for a wide range of phenomena associated with a reduced dimensionality and has therefore been studied extensively during recent decades. Examples include enhanced correlation effects such as charge-density wave (CDW) instabilities,[1–3] Mott insulator transitions,[4] and superconductivity.[5,6] The group 4 TMDC $1T$-$TiSe_2$ is of particular interest, as it is the only compound of this group exhibiting a CDW transition which is accompanied by a structural transition associated with the formation of a $(2\times2\times2)$ superlattice.[7,8] Even though the system has been the subject of a number of studies in the past, there is still an ongoing and lively discussion about the actual origin of this phase transition. Among others, Fermi-surface nesting,[8,9] a band-type Jahn-Teller mechanism,[3,7] and an excitonic insulator mechanism,[10] as well as combinations of these,[11] have been proposed. Recently also a competition between the CDW phase and a superconducting phase in copper doped $TiSe_2$ was observed.[5,6]

A distinction between the different models proposed so far is possible by a detailed inspection of peculiarities of the electronic structure particularly in the vicinity of the Fermi energy. For instance, a (band-type) Jahn-Teller mechanism is expected to be accompanied by an energy lowering of the Se $4p$ bands, which is associated with a Ti-Se bond shortening upon the transition into the CDW phase.[12] On the other hand, characteristics at the Γ point and the L point of the Brillouin zone are indicative of a phase transition driven by Fermi-surface nesting.[9] A thorough study of the $1T$-$TiSe_2$ band structure by means of angle-resolved photoelectron spectroscopy (ARPES) in the normal and in the CDW state is therefore a common and very efficient approach used to address the problem raised above.[7,11,13]

ARPES allows primarily for a spectroscopic access to the band structure associated with occupied electronic states. However, also the study of the properties of the unoccupied spectrum can contribute to the comprehensive understanding of the complex behavior of the TMDC compounds. In the past, the inverse photoemission technique (IPE) has been used to investigate the unoccupied band structure of the $1T$-$TiSe_2$ system.[14–16] It was possible to identify the Ti $3d^*$ band (conduction band 2 in this reference) in the ΓM direction in qualitative agreement with band-structure calculations.[9]

In this work we apply the angle-resolved two-photon photoelectron spectroscopy (AR-2PPE) to map the momentum-resolved unoccupied band structure of $1T$-$TiSe_2$. The 2PPE technique allows for a significantly higher energy resolution than the IPE technique.[17] Furthermore, in a stroboscopic (time-resolved) scheme, 2PPE (TR-2PPE) is capable of monitoring the ultrafast decay of bulk and surface electronic excitations at a temporal resolution of a few femtoseconds (10^{-15} s).[18] Such measurements can provide relevant insights into the decay mechanism of bulk decoupled electron states as has been shown, e.g., in the context of image potential states[18–22] and adsorbate excitations at noble-metal surfaces.[23–27]

Our 2PPE data proof the existence of a nondispersive unoccupied band at an energy of about 2.3 eV above the Fermi energy. We provide evidence that this band originates from excess titanium atoms embedded in the interlayer van der Waals gap of $TiSe_2$. The TR-2PPE experiments reveal a lifetime of the excess titanium atom excitation of about 7 fs, which is significantly longer than the measured lifetime of a Ti $3d^*$ band excitation within the $TiSe_2$ layers. This difference points to a considerable decoupling of the band from the bulk electronic structure and further supports our assignment to a state localized within the van der Waals gap. Our results show that an efficient decoupling of unoccupied states in resonance with bulk electronic states can emerge not only in front of a surface but also at specific sites located within a bulk.

II. EXPERIMENTAL DETAILS

The scheme of the experimental setup used in this work is shown in Fig. 1. ARPES and AR-2PPE as well as TR-2PPE experiments were performed in a magnetically shielded ultrahigh vacuum (UHV) chamber (base pressure below 5

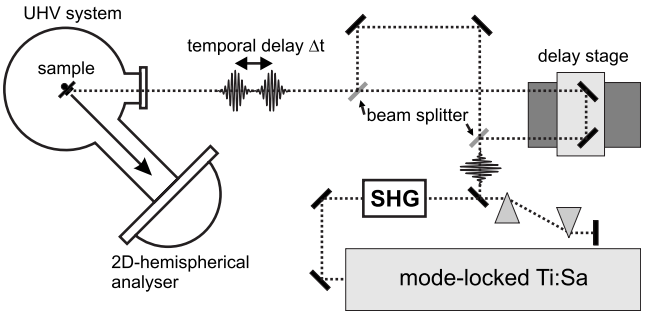

FIG. 1. Scheme of the experimental setup used for the 2PPE and TR-2PPE experiments.

$\times 10^{-11}$ mbar) using a hemispherical electron-energy analyzer ("PHOIBOS 150," SPECS, 150 mm radius). The analyzer is equipped with a two-dimensional (2D) detection unit which allows for parallel detection of the photoemitted electrons over a kinetic-energy range of typically 2 eV and an emission angle range of up to $\pm 13°$. The analyzer was set to an energy resolution of 20 meV and an angular resolution of 0.3°. The system is furthermore equipped with a low-energy electron diffraction (LEED) system which is used to check the surface quality and for alignment of the surface crystalline orientation prior to the photoemission experiments.

ARPES reference spectra have been recorded using the He-I emission (21.22 eV) of a gas discharge vacuum ultraviolet lamp. Next to initial and final states accessible in conventional photoemission experiments, 2PPE spectra contain in addition information about the unoccupied state distribution between Fermi energy and vacuum energy. Figure 2 illustrates the excitation scheme of a 2PPE process and the different electronic states contributing to the measured signal. The energy scale $E-E_F$ used in this work is determined from the kinetic energy E_{kin} of the photoelectrons analyzed in the spectrometer according to $E-E_F=E_{kin}+\Phi-h\nu$, with the work function Φ and the photon energy $h\nu$. For the 2PPE experiments we use the frequency converted output of two different-pulsed Ti:sapphire lasers: the AR-2PPE measurements are performed with the second harmonic (SH) and third harmonic (TH) of a narrow bandwidth laser system (laser 1, repetition rate: 80 MHz, bandwidth $\lessapprox 20$ meV). Under consideration of the electron analyzer setting the experimental setup using this laser system yields an overall energy resolution of $\cong 30$ meV. The wavelength of the laser light can be tuned continuously between 720 and 840 nm corresponding to photon energies of the SH light from $h\nu=2.95$ to 3.45 eV, and of the TH light from $h\nu=4.45$ to 5.15 eV.

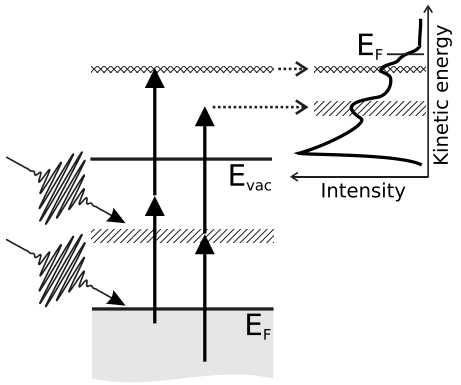

FIG. 2. Excitation scheme of the 2PPE process. The contribution of intermediate (hatched) and final (cross-hatched) states to the recorded spectrum is visualized.

For the time-resolved experiments we use a broad bandwidth laser system (laser 2, repetition rate: 76 MHz, bandwidth ≈ 90 meV), delivering frequency doubled light pulses of 28 fs temporal width at a photon energy of $h\nu=3.12$ eV. All TR-2PPE measurements are performed in the autocorrelation mode using identical, *p*-polarized laser pulses. The broader bandwidth of laser 2 leads to noticeable broadening of the spectral features in comparison to the AR-2PPE measurements. The data was phase averaged during acquisition using an electric-wobbling motor, thus eliminating interference contributions to the signal. A TR-2PPE scan consists of a series of $E(\boldsymbol{k}_\parallel)$-intensity maps recorded with the 2D energy analyzer at varying temporal delays Δt between the two pulses. Individual 2PPE autocorrelation traces from selected $E(\boldsymbol{k}_\parallel)$ areas can later be extracted from these intensity maps and then deconvoluted using calculated autocorrelation traces. For this purpose, the autocorrelation of a sech^2-shaped laser pulse is convoluted with a decreasing exponential. The time constant of the exponential corresponds to the lifetime of the unoccupied state. It is tuned for best fitting of the calculated to the experimental data.[28,29] This procedure finally yields in parallel a complete lifetime value data set $\tau(E,\boldsymbol{k}_\parallel)$, covering the complete experimentally accessible energy and momentum regime.[30] The laser-pulse duration at the sample surface, required for the deconvolution procedure, is determined by measurement of the 2PPE autocorrelation trace for excitation from the Cu(111) Shockley surface state.[31,32] For further illustration, the energy- and momentum-dependent lifetime variations are color coded and displayed in a two-dimensional $E-\boldsymbol{k}_\parallel$ representation as shown in Fig. 9(a).

The $1T$-$TiSe_2$ single crystals used for the experiments were grown by chemical vapor transport using iodine as a transport gas.[8] The crystals were grown at a temperature of 660 °C at a selenium excess of 3 $\mathrm{mg/cm^3}$. Such a procedure results in the formation of single crystals exhibiting structural homogeneous domains of up to about 3×3 $\mathrm{mm^2}$ suitable for photoemission experiments, however, on the costs of the crystal stoichiometry toward an enrichment with titanium atoms.[8,33,34] The preparation of a defined surface was performed by cleavage of the crystal under high-vacuum conditions and the subsequent removal of residual adsorbates by short annealing of the sample to 500 K under UHV conditions in the experimental chamber. The overall preparation procedure resulted in flat and shiny (0001) surfaces of the $TiSe_2$ samples yielding sharp LEED spots and well defined ARPES and AR-2PPE spectra. Surface impurities are known to modify the spectral weight of the electronic states of $1T$-$TiSe_2$ considerably[35,36] and can also completely quench the CDW transition as a result of a net charge transfer between adsorbate and compound. A reliable check of the surface quality in our experiments was the observation of the CDW transition by mapping characteristic changes[7,10,11,13,37] in the electronic structure at the $\bar{\mathrm{M}}$ point of the Brillouin

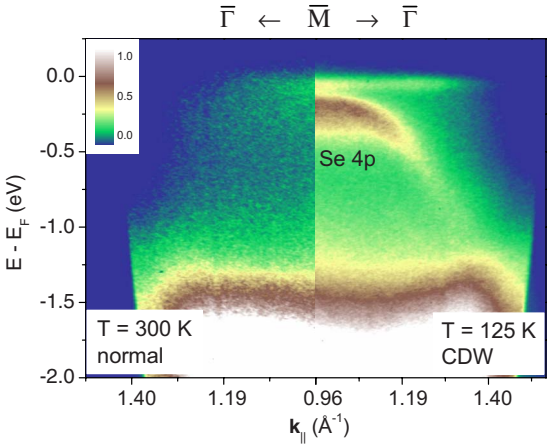

FIG. 3. (Color online) ARPES data at the $\bar{M}$ point of the Brillouin zone taken in the normal (300 K, left part) and CDW (125 K, right part) phase. The formation of the CDW ($2\times2\times2$) superlattice leads to a backfolding of the Se $4p$ bands, which appear at the $\bar{M}$ point. The conduction band, which is situated above the Fermi energy at room temperature, shifts into the occupied region during the phase transition. This leads to the appearance of the nondispersive feature right below the Fermi level upon cooling. The photon energy is $h\nu$=21.22 eV.

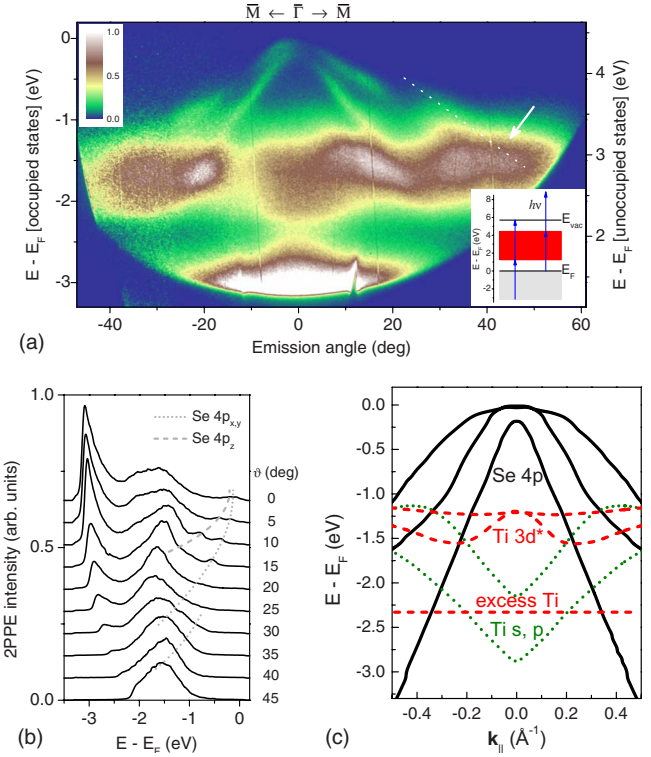

FIG. 4. (Color online) (a) AR-2PPE intensity map of pristine $1T$-$TiSe_2$, photon energy $h\nu$=4.43 eV. The map is composed of four partial spectra recorded at different polar angles of the sample relative to the analyzer axis. The partial spectra are shifted in angular direction for best correlation and blended at the seams using a special software ("SpecsComposer," SPECS, Version 1.0). Normalization is applied to match the intensity as homogeneous as possible. The labeling of the left axis displays the occupied states energies, the labeling of the right axis displays the unoccupied states energies of the 2PPE process. The colorscale corresponds to the mapping of the intensities. The inset shows the occupied and unoccupied states energy span that is sampled in this 2PPE experiment at the $\bar{\Gamma}$ point. (b) EDCs for selected emission angles extracted from the AR-2PPE intensity map. (c) Corresponding 2PPE-energy-reduced band scheme of $1T$-$TiSe_2$ following calculations from Refs. 9 and 43. Initial-state bands are shown in black, intermediate-state bands (red, dashed) have been shifted by $h\nu$=4.43 eV, final-state bands (green, dotted) have been shifted by $2h\nu$=8.86 eV. Intersections of different bands indicate possible direct transition within the 2PPE process. The nondispersive (unoccupied) band labeled "excess Ti" (dashed line) arises from excess Ti atoms located in the van der Waals gap of the layered crystal (Ref. 43).

zone using angle-resolved photoelectron spectroscopy (Fig. 3). The actual transition temperature of the samples into the CDW phase is (174 ± 3) K and was determined from the temperature dependence of the upper Se $4p$ band edge at the $\bar{\Gamma}$ point in reference to resistivity measurements by Rossnagel *et al.*,[7] where similarly prepared samples were used. This temperature value allows us to estimate the Ti excess concentration in the samples to about (1 ± 0.1)% based on reference data of Di Salvo *et al.*,[8] where the Ti excess atom content was referred to the observed CDW transition temperature in a systematical manner.

A work function of Φ=5.7 eV has been determined for several AR-2PPE experiments on the pristine $TiSe_2$ from the low-energy onset of the photoemission spectrum. This value is in good agreement with the results of previous measurements[16] and calculations.[38] For part of the experiments the $1T$-$TiSe_2$ surface was covered by a small amount of cesium from a SAES Getters source to reduce the surface work function. To inhibit the intercalation of the alkalis into the van der Waals gap of the $TiSe_2$ crystal, as reported in several works, we evaporated and performed these experiments at a sample temperature of 123 K.[39–42] For all photoemission experiments either a sheet of tantalum or a Cu(111) single crystal in electrical contact to the sample was used as Fermi energy reference.

III. RESULTS AND DISCUSSION

A. Spectroscopy of the unoccupied states of the $1T$-$TiSe_2$ compound

Figure 4 shows a composite AR-2PPE $E(\boldsymbol{k}_\parallel)$ intensity map recorded with the third harmonic of laser 1 (TH-2PPE) at a photon energy $h\nu$=4.43 eV and at four different polar angles of the sample with respect to the energy analyzer axis. This composite map is used for illustration only. The quantitative analysis of the data was performed using energy distribution curves (EDCs) deduced from the intensity maps as shown in Fig. 4(b) for different emission angles. Normal emission (0° emission angle) corresponds to electron emission from the $\bar{\Gamma}$ point. At a work function Φ=5.7 eV of the pristine $1T$-$TiSe_2$ sample, the used photon energy provides the spectroscopic access to an overall energy span of 3.16 eV [see inset of Fig. 4(a)]. This span covers an energy range for occupied states between −3.16 eV and the Fermi level E_F and an energy range for unoccupied states between 1.27 and 4.43 eV be-

tween E_F and the vacuum level. The energy scale used throughout this work is referred to the Fermi energy E_F.

The sharpest and therefore most distinctive features appearing in the TH-2PPE intensity map in Fig. 4(a) are the two parabolas at the top of the spectrum, exhibiting a strong, holelike dispersion in the vicinity of the $\bar{\Gamma}$ point. The parabolas are well known from conventional ARPES data (see Refs. 7, 11, 37, and 44) and can be attributed to the occupied Se $4p$ bands of the composite. The upper visible parabola corresponds to one of the two spin-orbit split Se $4p_x$, $4p_y$ valence bands.[45] The second split-off band is only barely visible at about +30° emission angle [indicated by the dashed line in Fig. 4(a)] and as a resonance feature at about +45° emission [arrow, see EDCs at different emission angles shown in Fig. 4(b)]. The lower parabola can be assigned to the Se $4p_z$ band.

The main spectral feature dominating the TH-2PPE data in Fig. 4 is the broad, weakly dispersive intensity band located in the occupied state-energy regime $E-E_F$ between −2.25 and −1.25 eV. In the following, we will show that this spectral feature has a complex origin, and contains contributions from five different bands. For a direct comparison with the experimental data, Fig. 4(c) shows an energy-band diagram of $1T$-$TiSe_2$ deduced from band-structure calculations in Ref. 9. These data cover the full-energy regime probed in our experiment. The data are completed by results from Ref. 43 which particularly consider the effect of defect states on the electronic structure. More recent band-structure calculations are also available from literature.[33,46–50] These data are, however, restricted with respect to the addressed energy range. The band energies and band dispersions provided by these data do not considerably deviate from the data from Ref. 9.

The data in Fig. 4(c) are shown in a representation that we refer to as a 2PPE energy-reduced band scheme. In this representation all energy bands which are potentially involved in the 2PPE process (initial-, intermediate-, and final-state bands) are projected to the initial-state energy level under consideration of the experimentally used photon energy, i.e., $h\nu$=4.43 eV in the present example. Final-state bands are therefore shifted down in energy by $2h\nu$, intermediate-state bands are shifted down by $h\nu$, and initial-state bands are not shifted at all. This representation allows for the comparison of experimental data and calculations in an intuitive and direct manner. In particular, band intersections in the reduced band scheme are indicative of potential resonant transitions within the 2PPE process.

Four main features are predicted by the calculations and the corresponding 2PPE energy-reduced band scheme: first of all, the above-mentioned parabolic Se $4p$ bands ($4p_x$, $4p_y$, and $4p_z$) which are shown in black (full line) and are clearly identified in the TH-2PPE intensity map. Second, the intermediate (unoccupied) states labeled in red (dashed line) which exhibit two distinct contributions. The two higher-lying energy levels are derived from a mixture of Ti $3d_{x^2-y^2}$, $3d_{xy}$, $3d_{xz}$, and $3d_{yz}$ orbitals and will in the following be referred to as Ti $3d^*$ bands in accordance with Ref. 48. The lower-lying nondispersive feature marks the energy of a band arising from the presence of Ti excess atoms in the van der

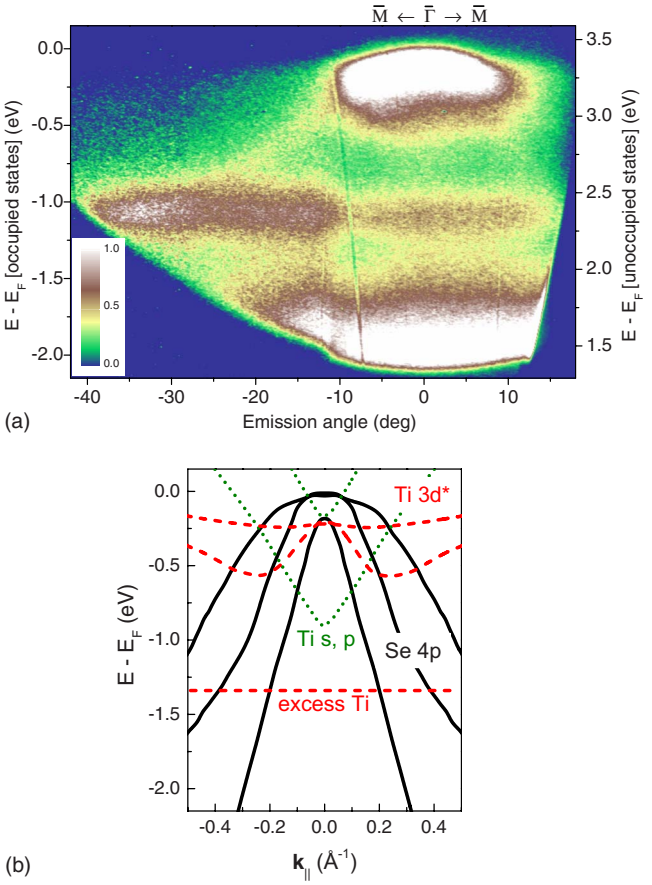

FIG. 5. (Color online) (a) AR-2PPE intensity map of $1T$-$TiSe_2$ covered by a small amount of cesium recorded with p-polarized laser light at a photon energy of $h\nu$=3.44 eV. The map is composed of three partial spectra, angularly shifted and blended as described in Fig. 4(a). The intensity of the two non-normal-emission spectra is amplified to enhance visibility of the Se $4p$ bands. Energy labeling corresponds to occupied states energy (left axis) and unoccupied states energy (right axis); (b) corresponding 2PPE energy-reduced band scheme ($h\nu$=3.44 eV).

Waals gaps of the layered crystal structure (excess Ti state) and was predicted by Pehlke and Schattke.[43] Finally, the two final-state bands marked in green (dotted line) are derived from high-energy titanium orbitals of s and p character.[9,16]

The broad intensity band in the experimental TH-2PPE data extends over an initial-state energy range from −2.25 to −1.25 eV. Note that these two energy values agree rather well with the energies of the Ti $3d^*$ band (−1.2 eV) and the excess Ti state (−2.3 eV) in the energy-reduced band scheme of Fig. 4(c). However, only the resonance features, due to the crossing of the Se $4p$ bands, can be assigned unambiguously from the experimental TH-2PPE data. AR-2PPE intensity maps recorded with second-harmonic light (SH-2PPE data) enable us to distinguish and identify further contributions to this intensity band.

Figure 5 shows a SH-2PPE intensity map recorded at a photon energy of $h\nu$=3.44 eV. As in the case of the TH-2PPE intensity map, Fig. 5(a) includes scales for occupied states energy (left) and unoccupied states energy (right). Figure 5(b) is the corresponding 2PPE related energy-reduced

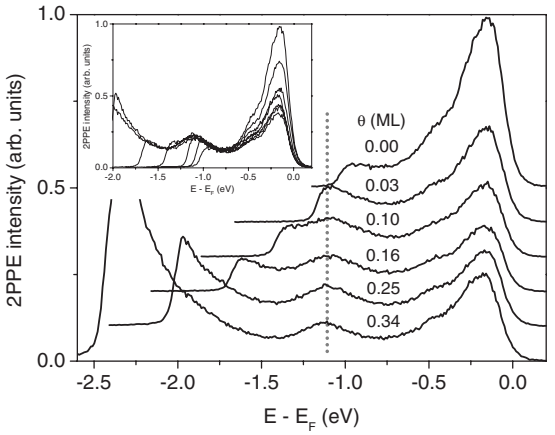

FIG. 6. Series of SH-2PPE EDC ($h\nu$=3.42 eV, normal emission) for different cesium coverages θ up to 0.34 ML. The position of the excess Ti band is emphasized by a dotted line. Inset: spectra plotted with non-normalized intensity. This representation clearly shows the appearance of the excess Ti state, as well as its insensitivity to the cesium coverage.

band scheme.[9,43] A meaningful 2PPE intensity map of a 1T-$TiSe_2$ sample recorded in the second-harmonic photon energy regime ($h\nu$=3.00 to 3.44 eV) requires a specific sample treatment which will be described and commented on in the following and prior to the discussion of the actual SH-2PPE data.

Because of the high work function value of 5.7 eV of the pristine 1T-$TiSe_2$ surface the accessible energy span in a 2PPE experiment recorded at $h\nu \approx 3$ to 3.5 eV is limited to a width of about 1.3 eV and below. To extend this energy span, the samples have been covered, in our study, with a small amount of cesium atoms [$\theta < 0.27$ monolayer (ML)], a procedure, which is well known to be very effective in reducing the surface work function.[38,51,52] Figure 6 shows 2PPE EDC of the $TiSe_2$ sample taken at increasing Cs coverages up to a maximum of 0.34 ML. The successive shift in the low-energy onset of the spectrum is indicative for the lowering of the surface work function.[53] It has to be emphasized that the interaction between alkali atoms and transition-metal dichalcogenides can be rather complex. Alkalis tend to intercalate into the van der Waals gap in between the crystal layers.[38,40–42] To thermally inhibit alkali intercalation, the sample temperature was therefore kept at 123 K during evaporation, as well as during the consequent experiments.[39,41,42]

Furthermore, electron transfer from the adsorbed alkali species to the substrate can give rise to a successive filling of the 1T-$TiSe_2$ bands and results in an increase in the electron binding energies.[52,54] In particular, the energy regime close to E_F, governed by the Se 4p bands, is considerably affected by the adsorbed Cs [see Fig. 6]. Three-peak fits to this spectral region [see Fig. 7(b)] show that the different spectral signatures exhibit an energy shift ΔE of up to 35 meV for the maximum Cs coverage used in this work. Additionally, the relative photoemission yield becomes clearly reduced due to the adsorption of Cs. In the quantitative analysis of the experimental data, this energy shift was taken into account. For other surface systems the appearance of new, surface-

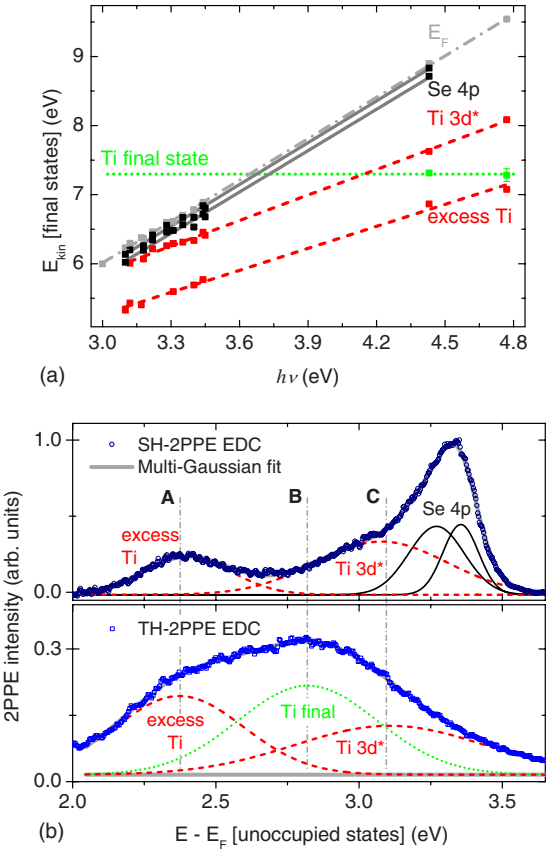

FIG. 7. (Color online) (a) Shift in the kinetic energy of the relevant spectral features observed in the 2PPE experiments as a function of the excitation photon energy (p-polarized). The respective slope of the shift is characteristic for the nature of the probed electron state (see text). This dependence allows us to assign the data points/lines labeled in red (dashed) to the unoccupied Ti 3d^* band and a state associated with the excess Ti atoms. (b) Comparison of an experimental SH- and TH-2PPE EDC ($h\nu$=3.44 eV and 4.43 eV, respectively, normal emission) with the result of a multiple Gaussian fit. Line style and color as per Fig. 4(c).

localized electron states due to the adsorption of alkalis has been reported.[51,55–59] In this 2PPE study such an alkali-derived state could not be observed. The peak at $E-E_F \approx -1.1$ eV ($E-E_F \approx 2.3$ eV unoccupied states energy) that becomes accessible due to the decrease in the work function is already present at zero Cs coverage (even so spectrally merely accessible at this coverage) as evidenced by the inset in Fig. 6. Even more (and in contrast to the low-energy part of the spectrum) this state is extremely robust against Cs adsorption and exhibits no detectable change in energy ($\Delta E < 15$ meV) and photoemissivity. A lowering of the work function by other adsorbates, i.e., nonalkalis, for instance, because of the contamination by the residual gas in the UHV chamber over days, will also render this feature visible with no significant changes. This insensitivity to modifications in the surface properties hints to a state that exhibits no or only negligible wave-function amplitude in the $TiSe_2$ top layer but that is buried underneath within the van der Waals gap of the crystalline structure. We will see later that this feature considerably contributes also to the broad intensity band in the

TH-2PPE intensity map of the noncesiated sample. The insensitivity of the 2PPE data to adsorbates/surface contaminations proofs that this state is not due to surface-localized states such as adsorbate states, surface states, or image potential states but that it is indeed an unoccupied electron state located within the bulk. Note also that a pronounced dependence of the photoemission yield on the polarization of the state is not observed as one would expect particularly in the case of surface states and image potential states.

Let us now consider in detail the SH-2PPE intensity map displayed in Fig. 5. At first glance the data exhibit the same general spectral features as the TH-2PPE spectrum: Parabolas exhibiting holelike dispersion just below the Fermi level because of photoemission from the Se $4p$ bands and additional (nondispersive) features at slightly lower energies that becomes fully accessible due to the work function reduction by the Cs. A closer inspection shows, however, clear differences in the spectral characteristics. The Se $4p$ signal in the SH spectrum appears blurred, yet strongly enhanced in the vicinity of the $\bar{\Gamma}$ point. Furthermore, the nondispersive feature appears to be much narrower than in the TH-2PPE spectrum. The energy-reduced band scheme in Fig. 5(b) gives an obvious explanation for both characteristics. The change in photon energy has shifted initial-, intermediate-, and final-state contributions with respect to each other in the initial-state energy projection. Therefore, for 2PPE excitation with $h\nu=3.44$ eV, the unoccupied excess Ti state is now expected to be rather isolated and well separated from the final-state titanium s and p orbitals (green, dotted parabolas). In fact, the energy of the excess Ti state as derived from the calculations fits rather well to the energy of the narrow band in the SH-2PPE data. This interpretation is corroborated by the robustness of the state against surface contamination indicating a localization within the van der Waals gap as expected for the Ti excess state. Furthermore, the Se $4p$ parabolas now show significant overlap with the intermediate Ti $3d^*$ band particularly at $\bar{\Gamma}$, and therefore explain the experimentally observed resonant enhancement and overall spectral broadening.

The quantitative analysis of AR-2PPE data recorded at a number of different photon energies supports our assignments and enables us to explicitly extract the respective band energies and dispersions from the experimental data. Figure 7(a) shows the kinetic-energy position (corresponding to the final-state energy) of all spectral features identified in the SH-2PPE maps at the $\bar{\Gamma}$ point as a function of the applied photon energy ($h\nu=3.00-3.45$ eV). This graph is completed by corresponding TH-2PPE data ($h\nu=4.40-4.75$ eV). The data points were extracted from the 2PPE EDCs deduced from the intensity maps and after subtraction of a secondary background mimicked by an exponential decay function. Peak positions were determined from multiple, sufficiently separated Gaussian fits. These fits delivered unambiguous peak energies from all SH-2PPE EDC. In the case of the TH-EDC the extraction of peak positions is, however, critical in the energy regime of the broad intensity band. Figure 7(b) compares a SH- and TH-EDC recorded at $h\nu=3.44$ and 4.43 eV, respectively, with the result of the multiple Gaussian fit. While two Gaussians are sufficient to fit the unoccupied

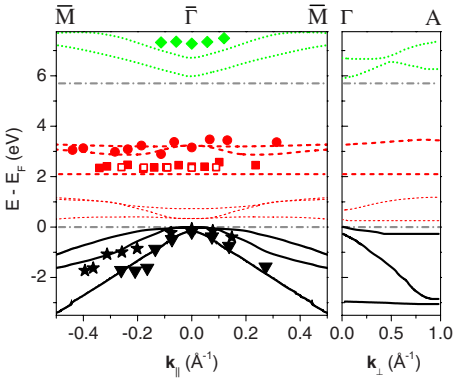

FIG. 8. (Color online) Left: calculated band structure along the ΓM direction ($\boldsymbol{k}_\parallel$) (Ref. 9) in comparison to the experimental results of this 2PPE study. The lower-lying red (dashed) line is the unoccupied nondispersive excess Ti atom band ($E-E_F=2.1$ eV, Ref. 43). Filled symbols correspond to experimental TH-2PPE data, open symbols correspond to SH-2PPE data. Right: calculated band-dispersion data perpendicular to the surface plane along the ΓA direction ($\boldsymbol{k}_\perp$).

features (dashed, peaks A and C) in the SH-EDC, a satisfactory fit to the dominating broad feature in the TH-EDC requires the assumption of a third Gaussian (dotted, peak B). We assign these three Gaussians to three different bands.

The slope of the peak positions in Fig. 7(a) allows one to distinguish initial-, intermediate-, and final-state contributions to the spectrum. A slope of $2\Delta h\nu$, two times the change in photon energy, is characteristic for an initial state, $\Delta h\nu$ is characteristic for an intermediate state and final states exhibit a vanishing slope.[60] The two parabolas in the vicinity of the Fermi edge, which we already assigned to the occupied (initial) Se $4p$ states, show indeed a slope of (2.0 ± 0.1) and (2.0 ± 0.2) as expected. They are shown in Fig. 7(a) by full black lines in correspondence to the color coding and line style used in the energy-reduced band schemata [Figs. 4(c) and 5(b)]. Another peak [labeled in red and dashed, C in Fig. 7(b)] which evolves slightly below the Se $4p$ parabolas in the SH-2PPE spectra as the photon energy increases exhibits a slope close to one (1.2 ± 0.1) and fades into the upper edge of the broad band feature in the TH-2PPE spectrum. Due to the energy of this state in comparison to the band-structure calculations, we assign the peak to the unoccupied Ti $3d^*$ bands. The deviation of the slope from one is likely due to the fit of the broad feature in the TH-EDC, as described above. Except for the Se $4p_z$ band all bands exhibit a small or even vanishing band dispersion in $\boldsymbol{k}_\perp$, because of the weak coupling between the $TiSe_2$ layers (see band-structure calculations[9] shown in Fig. 8). Therefore, the experimentally determined photon-energy slopes are not affected by the $\boldsymbol{k}_\perp$ dispersion as reported before for instance in the case of a resonant interband excitation in Ag(111).[61,62] With respect to the Se $4p_z$ band the observed slope of two just confirms the unambiguous assignment on the basis of the $\boldsymbol{k}_\parallel$ dispersion and the comparison with 1PPE measurements and the band-structure calculation. In this case the pronounced $\boldsymbol{k}_\perp$ dispersion does not seem to affect the photon-energy dependence of the 2PPE signature. The data points at the lowest energy values [also shown in red and dashed, A in Fig. 7(b)] corre-

spond to the separated nondispersing band in the SH-2PPE intensity map. These data points also exhibit a slope close to one (1.1 ± 0.1) and further support our previous assignment to the nondispersive unoccupied excess Ti atom state.

Let us finally consider the slope of the center Gaussian fitted to the broad band feature in the TH-2PPE EDC [Fig. 7(b)] and displayed in Fig. 7(a) in green (dotted line). This peak does not exhibit any change in position with excitation energy and is therefore characteristic for a final-state contribution. Extrapolation of these data to the second-harmonic photon-energy regime (3.0–3.5 eV) [see also Fig. 7(a)] shows that this state is located well above the final-state cutoff energies in these spectra (labeled by the gray dashed-dotted line) and therefore cannot contribute to the SH-2PPE signal. In comparison with the reduced band scheme the energy of this state fits approximately to the energy of the upper of the two final-state Ti bands of *s* and *p* character. We do not observe any contribution of a second final-state band in any of the 2PPE data.

In a similar manner, peak positions of 2PPE EDC curves at different, finite $\boldsymbol{k}_{\parallel}$ values along the ΓM direction have been evaluated. The results are summarized in Fig. 8 and are directly compared with the band-structure calculations from Refs. 9 and 43. The first conduction band of the $TiSe_2$ compound, exhibiting a Ti $3d^*$ and Ti $3d_{z^2}$ character with admixtures of Se $4p$ bands,[48] is located at an energy between 0 and 1 eV above the Fermi level and therefore experimentally not accessible with the photon energies available for our 2PPE study. For the upper unoccupied Ti $3d^*$ band (full red circles) the experimental data show only a weak dispersion and an energy of $E-E_F=(3.0 \pm 0.1)$ eV at the $\bar{\Gamma}$ point, as derived from Fig. 7. This result is in good agreement with the calculated band structure, which yields a corresponding value of 3.2 eV (Refs. 9 and 49) and 3.1 eV (Ref. 48), respectively. For comparison, in previous IPE studies a value of 3.1 eV (Ref. 15) to 3.2 eV (Ref. 16) was reported.

The data points located approximately 0.7 eV below the Ti $3d^*$ band (open and filled red squares) correspond to the band that we assigned to the excess Ti atom states. The absence of any dispersion in the experimental data supports the localized character of this state and an energy of $E-E_F=(2.3 \pm 0.1)$ eV agrees well with the calculated value of 2.1 eV.[43] The energy of the state is rather close to the regular Ti $3d^*$ bands which is not very surprising considering the rather similar octahedral coordination site proposed for both Ti species, within the regular $TiSe_2$ layers and within the van der Waals gap of the crystal, respectively.[38,41] At first glance it may be surprising that the Ti excess peak shows up in the spectra at a significant intensity even though only 1% of all Ti atoms contribute to this signal. However, as we will see later, this state exhibits a rather long lifetime which enhances the probability for the second 2PPE excitation step and consequently the efficiency of the overall 2PPE process.

The observed final-state energy in the 2PPE experiment (green diamonds) agrees within about 0.6 eV with the predictions for the Ti band of *s* and *p* character.[9] This result is, however, worse than for the other bands. Furthermore, the expected band dispersion cannot be confirmed experimentally.

We now comment in more detail on the actual origin of the Ti excess atoms in our samples. Pehlke and Schattke considered in their theoretical work titanium atoms that have been removed from a crystalline layer, leaving vacancies within the layer, and occupying empty sites within the interlayer van der Waals gap.[43] These kinds of defects have been referred to as "Frenkel-type defects," characterized by additional occupied and unoccupied localized states. The results of their calculations give evidence for a vacancy state at $E-E_F=-1.5$ eV, and states localized at the Ti excess atom at energies of −7, 0.5, and 2.1 eV. The existence of the nondispersive vacancy state at an energy of −1.5 eV has been previously observed in a conventional photoemission experiment.[43,45] Here, we present experimental evidence for the unoccupied state of the Ti excess atom at an energy of 2.1 eV. From a preparational point of view, it is likely that the Ti excess atoms were embedded into the van der Waals gap during the growth process of the $TiSe_2$ crystal. Note that $TiSe_2$ tends to grow at a surplus of titanium atoms, even if a compensating selenium excess has been applied for the growth process.[8,33,63] Such a Ti surplus (approximately 1% for the samples used in this work) guarantees the growth of large $TiSe_2$ single crystals required for the photoemission experiments as discussed already in the experimental section. The appearance of vacancies is therefore not expected in our case. Experimentally we neither observe a vacancy state at −1.5 eV in conventional ARPES, nor in the 2PPE intensity maps (Figs. 4 and 5) supporting this view.

In the following section we will focus on the ultrafast decay dynamics associated with the population of the unoccupied Ti $3d^*$ band and the excess Ti atom state. Both bands originate from titanium $3d$ orbitals. Since the unoccupied state associated with the excess Ti is much more strongly localized at the corresponding atoms, one can expect a clear distinction between both excitations with respect to their lifetime.

B. Decay dynamics of Ti-localized unoccupied states

The time-resolved experiments were performed using the second-harmonic light of laser 2 ($h\nu=3.12$ eV, 28 fs). The left part of Fig. 9(a) shows a SH-2PPE intensity map from a sample recorded with this light source. Note that for these measurements the work function of the $1T$-$TiSe_2$ sample was lowered by 1.2 eV by the adsorption of cesium ($\theta=0.27$ ML). Clearly visible and marked by the dotted box is the nondispersing excess Ti atom state at an energy of about 2.3 eV. The Se $4p$ band just below the Fermi edge shows, at this photon energy, a distinct structure exhibiting a maximum at about −4° emission angle and marked in the figure by a dotted ellipse. This intensity maximum arises from the resonant excitation of the weakly dispersing Ti $3d^*$ intermediate-state band from the strongly downward dispersing Se $4p$ initial-state band at finite $\boldsymbol{k}_{\parallel}$ values [see Fig. 9(b), excitation path i]. At a photon energy of $h\nu = 3.12$ eV a resonant excitation is not possible at the $\bar{\Gamma}$ point [see Figs. 9(a) and 9(b), excitation path ii], due to the higher energetic separation of the Ti $3d^*$ and Se $4p$ bands. The 2PPE process enables us to selectively address two distinct unoccupied states of the

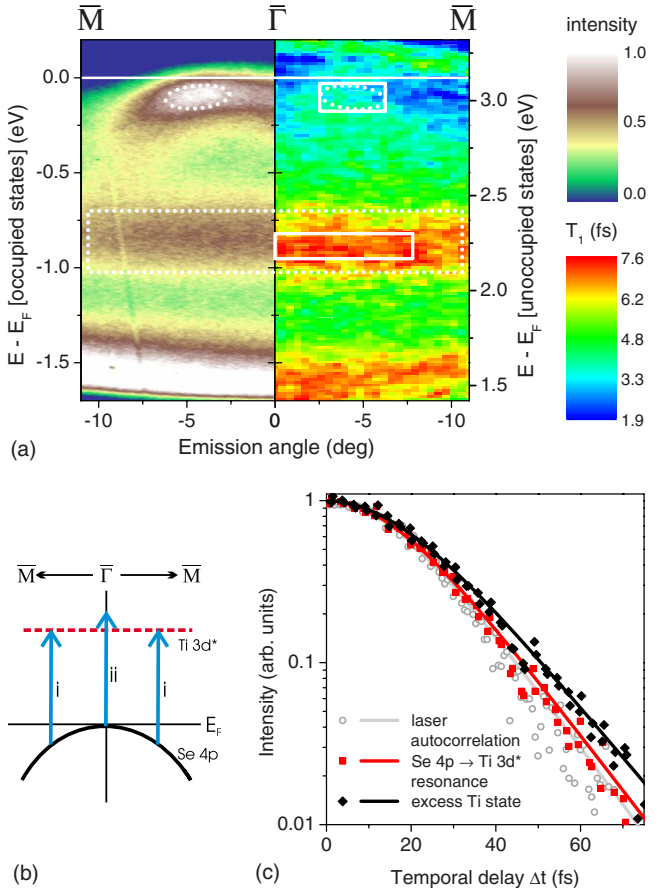

FIG. 9. (Color online) (a) Left: SH-2PPE spectrum of $1T$-$TiSe_2$ recorded with laser 2 at $h\nu$=3.12 eV (p-polarization). Right: corresponding lifetime map deduced from a time-resolved 2PPE scan. Lifetimes are color coded as labeled in the inset. The left scale shows occupied states energy and the right scale unoccupied states energy with respect to E_F. The dotted lines highlight the distinct spectral features. The full boxes mark the integration areas that have been used to extract the 2PPE autocorrelation traces shown in (c). (b) Scheme of the resonant excitation pathways at $h\nu$=3.12 eV. (c) Comparison of the 2PPE autocorrelation traces related to excess Ti atom state and Ti $3d^*$ band, respectively. The laser autocorrelation is also shown.

$1T$-$TiSe_2$ compound, both derived from Ti $3d$ orbitals. In the following we will focus on the population lifetime T_1 of these two unoccupied states, Ti $3d^*$ and Ti excess state, as probed by means of time-resolved 2PPE.

The right part of Fig. 9(a) also shows a color-coded lifetime map derived from a TR-2PPE scan as described in detail in Sec. II and in Refs. 29 and 30. A blue, green, and red color coding corresponds here to short, medium, and the longest lifetimes measured within this experiment, respectively. The actual lifetime values have been deduced from the measured 2PPE autocorrelation traces following an analysis procedure suggested in Ref. 28 and under the assumption of rapid-dephasing conditions within both excitation steps of the 2PPE process.[64,65] The lifetime map covers the identical energy and momentum range shown in the 2PPE intensity map on the left of Fig. 9(a). Once again the $E(\boldsymbol{k}_{\parallel})$ areas related to the excitation of the excess Ti atom state and the Ti $3d^*$ band are marked by the dotted box and the dotted ellipse, respectively. Evident from these data is a distinct maximum in the unoccupied state population lifetime of about 7 fs at the energy of the excess Ti atom state, which is independent of the probed momentum vector $\boldsymbol{k}_{\parallel}$. By contrast, in the energy region of the Se $4p$ band, autocorrelation traces are measured, which closely follow the laser autocorrelation. In the lifetime map this behavior gives rise to the pronounced minimum, mimicking the parabolic downward dispersion of the Se $4p$ band in correspondence to the 2PPE spectroscopy data. Only at the $E(\boldsymbol{k}_{\parallel})$ area, which is indicative for the resonant excitation of the Ti $3d^*$ band (see dotted ellipse), the color coding of the lifetime map points to an increase in the measured lifetime to values of about 3.0 fs. We assign this local maximum to the actual population lifetime T_1 of the Ti $3d^*$ band. On the other hand, the minimum lifetime value along the rest of the Se $4p$ parabola, i.e., outside the area of the resonant excitation, arises from the off-resonant character of the 2PPE process.[31,32]

To illustrate the difference in the depopulation dynamics between excess Ti atom state and Ti $3d^*$ band, we compare in Fig. 9(c) the corresponding 2PPE autocorrelation traces. These traces have been generated by signal integration of the respective areas marked in the lifetime map in Fig. 9(a) by full boxes. The result of the quantitative analysis of the two Ti autocorrelation traces is displayed as a full line. For reference the laser autocorrelation has also been added to Fig. 9(c) (open symbols), which has been determined from the time-resolved 2PPE signal of the Shockley surface state of a well-prepared Cu(111) single-crystal surface.[31,32] The broadening of both unoccupied Ti state autocorrelation traces in comparison to the laser autocorrelation is indicative for the finite lifetime T_1 of the Ti-intermediate states involved in the 2PPE process. The quantitative analysis delivers a lifetime $T_1=(7.1\pm3.3)$ fs for the excess Ti atom state and a lifetime $T_1<3$ fs for the Ti $3d^*$ band. The population decay of the excess Ti state happens on a time scale which is about 2.5 times slower than the population decay of the Ti $3d^*$ band.

We suggest that the difference in the population lifetime of the two unoccupied Ti states arises from the characteristic differences in the electronic coupling of the corresponding layer and interlayer titanium sites to the $TiSe_2$ bulk electronic structure. As mentioned above, both the regular Ti atoms embedded within the crystal layers (layer Ti atoms), as well as, the excess Ti atoms located within the van der Waals gap, exhibit octahedral coordination sites with respect to the selenium atoms.[38,41] Furthermore, the unoccupied states probed in our time-resolved experiment are very similar with respect to the involved atomic orbitals. The inelastic population decay of these states, which is mainly governed by the coupling to the electronic environment, is, however, expected to differ significantly. Within the crystal layers the large orbital overlap with the layer electronic structure provides a multitude of efficient channels for the inelastic decay of the unoccupied Ti $3d^*$ band via electron-hole pair excitation. These decay channels are less efficient for the spatially decoupled excess Ti state. The experimentally observed increase in the lifetime of the Ti excess state is a direct consequence of this decoupling.

Efficiently decoupled unoccupied states in solid-state systems have been observed particularly in the context of

surface-localized unoccupied states in the past: examples are, for instance, image potential states[18–22] and adsorbate resonances on noble-metal surfaces.[23–27] The characteristic lifetimes of these states, which are also governed by the coupling to the substrate electronic structure, cover the low femtosecond to picosecond regime. The comparatively long lifetime of the Ti excess atom state, in comparison to the layer Ti atoms shows that in a similar manner a stabilization of electronic resonances is also possible within the bulk.

IV. CONCLUSION

In this work, we performed an angle-resolved two-photon photoemission study of the transition-metal dichalcogenide $1T$-$TiSe_2$. In addition to the well-known spectral signatures of the occupied Se $4p$ valence bands, we are able to identify two different unoccupied bands in the system. The Ti $3d^*$ conduction band, which has been observed before in a IPE experiment, and a nondispersive band, which we assign to the excitation of excess Ti atoms within the van der Waals gap of the crystal. In a theoretical study,[43] this band was predicted before. The present paper provides experimental proof for the existence of this band.

Time-resolved 2PPE data give insight into the coupling efficiency of the Ti excess state to the electronic environment. In comparison to the interlayer Ti $3d^*$ band we observe an increase in the population lifetime of the excess Ti state by more than a factor of 2 up to a value of $T_1 = (7.1 \pm 3.3)$ fs. This difference is attributed to the reduction in the coupling of the excess Ti state to the electronic band structure of the $TiSe_2$ layers. Our results particularly show that besides surface-localized unoccupied states bulk-embedded states can exhibit an efficient decoupling from the residual decay channels.

ACKNOWLEDGMENTS

The authors would like to thank M. Aeschlimann for providing his photoemission experiment for these studies, L. Kipp and W. Krüger for providing the crystals used throughout this work, and K. Rossnagel for helpful discussions. Financial support for F. Steeb and S. Mathias was provided by the Deutsche Forschungsgemeinschaft under Grant No. DFG GRK 792 "Nichtlineare Optik und Ultrakurzzeitphysik."

*wiesenmayer@physik.uni-kiel.de

[1] E. Doni and R. Girlanda, in *Electronic Structure and Electronic Transitions in Layered Materials*, edited by V. Grasso (Reidel, Dordrecht, 1986), pp. 1–171.
[2] M. Grioni and J. Voit, in *Electron Spectroscopies Applied to Low-Dimensional Materials*, edited by H. P. Hughes and H. I. Starnberg (Kluwer, Dordrecht, 2000), Chap. 5, pp. 209–281.
[3] O. Anderson, G. Karschnick, R. Manzke, and M. Skibowski, Solid State Commun. **53**, 339 (1985).
[4] L. Perfetti, P. A. Loukakos, M. Lisowski, U. Bovensiepen, H. Berger, S. Biermann, P. S. Cornaglia, A. Georges, and M. Wolf, Phys. Rev. Lett. **97**, 067402 (2006).
[5] G. Li, W. Z. Hu, D. Qian, D. Hsieh, M. Z. Hasan, E. Morosan, R. J. Cava, and N. L. Wang, Phys. Rev. Lett. **99**, 027404 (2007).
[6] D. Qian, D. Hsieh, L. Wray, E. Morosan, N. L. Wang, Y. Xia, R. J. Cava, and M. Z. Hasan, Phys. Rev. Lett. **98**, 117007 (2007).
[7] K. Rossnagel, L. Kipp, and M. Skibowski, Phys. Rev. B **65**, 235101 (2002).
[8] F. J. Di Salvo, D. E. Moncton, and J. V. Waszczak, Phys. Rev. B **14**, 4321 (1976).
[9] A. Zunger and A. J. Freeman, Phys. Rev. B **17**, 1839 (1978).
[10] H. Cercellier *et al.*, Phys. Rev. Lett. **99**, 146403 (2007).
[11] T. E. Kidd, T. Miller, M. Y. Chou, and T.-C. Chiang, Phys. Rev. Lett. **88**, 226402 (2002).
[12] M. H. Whangbo and E. Canadell, J. Am. Chem. Soc. **114**, 9587 (1992).
[13] T. Pillo, J. Hayoz, H. Berger, F. Lévy, L. Schlapbach, and P. Aebi, Phys. Rev. B **61**, 16213 (2000).
[14] W. Drube, I. Schäfer, G. Karschnick, and M. Skibowski, Phys. Rev. B **30**, 6248 (1984).
[15] D. Straub, M. Skibowski, F. J. Himpsel, and W. Drube, Phys. Rev. B **31**, 8254 (1985).
[16] W. Drube, I. Schäfer, and M. Skibowski, J. Phys. C **20**, 4201 (1987).
[17] T. Fauster and W. Steinmann, *Photonic Probes of Surfaces, Electromagnetic Waves: Recent Developments in Research* (North-Holland, Amsterdam, 1995), Vol. 2, Chap. 8, pp. 347–411.
[18] R. W. Schoenlein, J. G. Fujimoto, G. L. Eesley, and T. W. Capehart, Phys. Rev. Lett. **61**, 2596 (1988).
[19] U. Höfer, I. L. Shumay, C. Reuß, U. Thomann, W. Wallauer, and T. Fauster, Science **277**, 1480 (1997).
[20] J. D. McNeill, R. L. Lingle, N.-H. Ge, C. M. Wong, R. E. Jordan, and C. B. Harris, Phys. Rev. Lett. **79**, 4645 (1997).
[21] M. Weinelt, C. Reuss, M. Kutschera, U. Thomann, I. L. Shumay, T. Fauster, U. Höfer, F. Theilmann, and A. Goldmann, Appl. Phys. B **68**, 377 (1999).
[22] K. Ertel, U. Kohl, J. Lehmann, M. Merschdorf, W. Pfeiffer, A. Thon, S. Voll, and G. Gerber, Appl. Phys. B **68**, 439 (1999).
[23] M. Bauer, S. Pawlik, and M. Aeschlimann, Phys. Rev. B **55**, 10040 (1997).
[24] S. Ogawa, H. Nagano, and H. Petek, Phys. Rev. Lett. **82**, 1931 (1999).
[25] E. Knoesel, A. Hotzel, T. Hertel, M. Wolf, and G. Ertl, Surf. Sci. **368**, 76 (1996).
[26] C. Frischkorn and M. Wolf, Chem. Rev. **106**, 4207 (2006).
[27] J. P. Gauyacq, A. G. Borisov, and M. Bauer, Prog. Surf. Sci. **82**, 244 (2007).
[28] J. P. Gauyacq and A. K. Kazansky, Phys. Rev. B **72**, 045418 (2005).
[29] M. Wiesenmayer, M. Bauer, S. Mathias, M. Wessendorf, E. V. Chulkov, V. M. Silkin, A. G. Borisov, J.-P. Gauyacq, P. M. Echenique, and M. Aeschlimann, Phys. Rev. B **78**, 245410 (2008).
[30] S. Mathias, A. Ruffing, F. Deicke, M. Wiesenmayer, M. Aeschlimann, and M. Bauer, Phys. Rev. B **81**, 155429 (2010).
[31] T. Hertel, E. Knoesel, M. Wolf, and G. Ertl, Phys. Rev. Lett. **76**,

535 (1996).
[32] F. Steeb, S. Mathias, A. Fischer, M. Wiesenmayer, M. Aeschlimann, and M. Bauer, New J. Phys. **11**, 013016 (2009).
[33] J. A. Wilson, Phys. Status Solidi B **86**, 11 (1978).
[34] D. K. G. de Boer, C. F. van Bruggen, G. W. Bus, R. Coehoorn, C. Haas, G. A. Sawatzky, H. W. Myron, D. Norman, and H. Padmore, Phys. Rev. B **29**, 6797 (1984).
[35] G. Karschnick, O. Anderson, W. Drube, and M. Skibowski, Surf. Sci. **155**, 46 (1985).
[36] J. Rasch, T. Stemmler, and R. Manzke, J. Alloys Compd. **442**, 262 (2007).
[37] N. G. Stoffel, S. D. Kevan, and N. V. Smith, Phys. Rev. B **31**, 8049 (1985).
[38] C. Ramírez, R. Adelung, R. Kunz, L. Kipp, and W. Schattke, Phys. Rev. B **71**, 035426 (2005).
[39] C. Pettenkofer, W. Jaegermann, A. Schellenberger, E. Holub-Krappe, C. A. Papageorgopoulos, M. Kamaratos, and A. Papageorgopoulos, Solid State Commun. **84**, 921 (1992).
[40] H. I. Starnberg, H. E. Brauer, and H. P. Hughes, in *Electron Spectroscopies Applied to Low-Dimensional Materials*, edited by H. P. Hughes and H. I. Starnberg (Kluwer, Dordrecht, 2000), Chap. 2, pp. 41–98.
[41] S. E. Stoltz, H. I. Starnberg, and L. J. Holleboom, Phys. Rev. B **71**, 125403 (2005).
[42] H. I. Starnberg, H. E. Brauer, and V. N. Strocov, Surf. Sci. **384**, L785 (1997).
[43] E. Pehlke and W. Schattke, Z. Phys. B **66**, 31 (1987).
[44] S. Negishi *et al.*, Physica B **383**, 155 (2006).
[45] E. Pehlke, W. Schattke, O. Anderson, R. Manzke, and M. Skibowski, Phys. Rev. B **41**, 2982 (1990).
[46] H. Isomäki, J. von Boehm, and P. Krusius, J. Phys. C **12**, 3239 (1979).
[47] N. Suzuki, A. Yamamoto, and K. Motizuki, Solid State Commun. **49**, 1039 (1984).
[48] C. M. Fang, R. A. de Groot, and C. Haas, Phys. Rev. B **56**, 4455 (1997).
[49] C. del Pilar Ramírez García, Ph.D. thesis, Christian-Albrechts-Universität zu Kiel, 2003.
[50] F. Clerc, C. Battaglia, H. Cercellier, C. Monney, H. Berger, L. Despont, M. G. Garnier, and P. Aebi, J. Phys.: Condens. Matter **19**, 355002 (2007).
[51] N. Fischer, S. Schuppler, T. Fauster, and W. Steinmann, Surf. Sci. **314**, 89 (1994).
[52] W. Jaegermann, C. Pettenkofer, A. Schellenberger, C. A. Papageorgopoulos, M. Kamaratos, D. Vlachos, and Y. Tomm, Chem. Phys. Lett. **221**, 441 (1994).
[53] The cesium coverage was calibrated by monitoring the work-function decrease during evaporation at room temperature. We followed a procedure described in Ref. 66 and references therein, especially Refs. 67 and 68. We assigned the transition from linear to nonlinear work-function decrease to a coverage of 0.4 ML and assumed a linear behavior of the cesium coverage with respect to the work function below 0.4 ML.
[54] C. Ramírez and W. Schattke, Surf. Sci. **482-485**, 424 (2001).
[55] D. Tang and D. Heskett, Phys. Rev. B **47**, 10695 (1993).
[56] D. A. Arena, F. G. Curti, and R. A. Bartynski, Phys. Rev. B **56**, 15404 (1997).
[57] W. Jacob, E. Bertel, and V. Dose, Phys. Rev. B **35**, 5910 (1987).
[58] H. Nielsen and W. Thowladda, Surf. Sci. **284**, L426 (1993).
[59] K.-H. Frank, H.-J. Sagner, and D. Heskett, Phys. Rev. B **40**, 2767 (1989).
[60] N. Fischer, S. Schuppler, R. Fischer, T. Fauster, and W. Steinmann, Phys. Rev. B **43**, 14722 (1991).
[61] S. Pawlik, R. Burgermeister, M. Bauer, and M. Aeschlimann, Surf. Sci. **402-404**, 556 (1998).
[62] N. Pontius, V. Sametoglu, and H. Petek, Phys. Rev. B **72**, 115105 (2005).
[63] H. Isomäki and J. von Boehm, J. Phys. C **14**, L75 (1981).
[64] M. Weida, S. Ogawa, H. Nagano, and H. Petek, J. Opt. Soc. Am. B **17**, 1443 (2000).
[65] M. Merschdorf, C. Kennerknecht, and W. Pfeiffer, Phys. Rev. B **70**, 193401 (2004).
[66] M. Boehme, Ph.D. thesis, Christian-Albrechts-Universität zu Kiel, 1998.
[67] S. Kennou, S. Ladas, and C. Papageorgopoulos, Surf. Sci. **152-153**, 1213 (1985).
[68] C. A. Papageorgopoulos, Surf. Sci. **75**, 17 (1978).